

Apparent quasar disc sizes in the “bird’s nest” paradigm

P. Abolmasov

¹ Tuorla Observatory, University of Turku, Väisäläntie 20, FI-21500 Piikkiö, Finland

² Sternberg Astronomical Institute, Moscow State University, Universitetsky pr., 13, Moscow 119992, Russia,
e-mail: pavel.abolmasov@gmail.com

ABSTRACT

Context. Quasar microlensing effects make it possible to measure the accretion disc sizes around distant supermassive black holes that are still well beyond the spatial resolution of contemporary instrumentation. The sizes measured with this technique appear inconsistent with the standard accretion disc model. Not only are the measured accretion disc sizes larger, but their dependence on wavelength is in most cases completely different from the predictions of the standard model.

Aims. We suggest that these discrepancies may arise not from non-standard accretion disc structure or systematic errors, as it was proposed before, but rather from scattering and reprocessing of the radiation of the disc. In particular, the matter falling from the gaseous torus and presumably feeding the accretion disc may at certain distances become ionized and produce an extended halo that is free from colour gradients.

Methods. A simple analytical model is proposed assuming that a geometrically thick translucent inflow acts as a scattering mirror changing the apparent spatial properties of the disc. This inflow may be also identified with the broad line region or its inner parts.

Results. Such a model is able to explain the basic properties of the apparent disc sizes, primarily their large values and their shallow dependence on wavelength. The only condition required is to scatter a significant portion of the luminosity of the disc. This can easily be fulfilled if the scattering inflow has a large geometrical thickness and clumpy structure.

Key words. accretion, accretion discs – quasars: general – scattering – gravitational lensing: micro

1. Introduction

While the mechanisms responsible for the spectral energy distributions of bright active galactic nuclei are more or less understood in the framework of standard disc accretion theory, there are certain observational results that lack unambiguous interpretation. One of the most puzzling is the behaviour of the accretion disc sizes measured through microlensing effects. Pooley et al. (2007) have found the observed disc sizes to exceed the standard theory predictions by one-two orders of magnitude. Later, in Morgan et al. (2010), this result was qualitatively confirmed, but the real value of discrepancy appeared to be smaller – about a factor of several. Even more important is that the wavelength dependence of the radius seems to deviate generally from the expected standard theory scaling. For a multi-temperature disc with a power-law temperature dependence on radius, $T \propto R^{-p}$, the apparent radius should scale as $R \propto \lambda^{1/p}$. In particular, for a standard disc, $T \propto R^{-3/4}$ (Shakura & Sunyaev 1973) and $R \propto \lambda^{4/3}$. Blackburne et al. (2011) find that for the larger part of their 12-object sample, the apparent disc sizes in the UV/optical range (0.1–1 μ m) show much weaker dependence on wavelength. An evident solution is to assume steeper temperature profile, but there seem to be no physically motivated models able to reproduce the very small temperature slopes $p > 1$ (see also discussion in Floyd et al. (2009)). Another solution is to assume that the measured spatial scales are not representative of the accretion disc itself. For instance, Yan et al. (2014) suggest that a sub-parsec black hole binary model may reproduce some of the observational results. In this case, the observed size of the emit-

ting region is close to the separation of the binary that does not depend on wavelength.

It seems that this large-radius problem is typical for lower mass black holes ($M \lesssim 10^9 M_\odot$), while the discs of the most massive supermassive black holes better conform to the standard disc theory (see Fig. 4 in Abolmasov & Shakura (2012)). Because the sample of lensed quasars is biased towards brighter objects, one can suggest that smaller black holes should have higher Eddington ratios, i.e. higher mass accretion rates in Eddington units. Accretion upon smaller black holes should probably be even super-Eddington (Shakura & Sunyaev 1973). Super-Eddington mass accretion is expected to lead to the formation of outflows that are able to cover the inner parts of the visible disc. In Abolmasov & Shakura (2012), we consider the spatial properties of quasar accretion discs affected by a spherically symmetric scattering envelope formed by the wind produced by super-Eddington accretion. However, in such a model, the mass accretion rates required seem to be unexpectedly large, $\dot{m} > 10^3$, where \dot{m} is mass accretion rate in dimensionless units,

$$\dot{m} = \frac{\dot{M}c^2}{L_{\text{Edd}}} = \frac{\dot{M}\kappa c}{4\pi GM}, \quad (1)$$

where $L_{\text{Edd}} = \frac{4\pi GMc}{\kappa}$ is the Eddington luminosity and κ is the (presumably, Thomson) opacity of the medium. The black hole masses inferred are inconsistent with the virial mass estimates (Abolmasov & Shakura 2013). There are no indications for mass accretion rates this high even in the brightest AGN while some estimates around $\dot{m} \sim 100$ exist (see for example Collin et al. 2002). For near-Eddington mass accretion rates, the super-Eddington region is small and the outflows are too fast ($v \sim \dot{m}^{-1/2}$) and, hence, the optical depths are too small.

Send offprint requests to: Pavel Abolmasov, e-mail: pavel.abolmasov@gmail.com

This actually means that if one wants to reproduce the observed quasar sizes with the outflow-based model, the outflows either should be bound (and thus be disqualified as outflows) or possess nearly zero total mechanical energy (parabolic motion). The latter seems unrealistic because some process is required to ensure the outflow has the kinetic energy that is exactly equal to its potential energy. This problem is eliminated if one assumes that an *inflow* rather than an outflow is responsible for the formation of the scattering envelope. In this case, nearly parabolic motion is a natural outcome of energy conservation if the energy is lost at dynamical or longer timescales. The infalling matter may scatter or reprocess the radiation of the disc, thus making the effective size of the disc larger.

There is another line of evidence for the existence of scattering material around supermassive black hole accretion discs, which comes from the broad emission-line regions (BLRs). Broad components of emission lines in quasars and other active galactic nuclei (AGNs) are currently believed to be formed in a clumpy partially ionized gas in a geometrically thick disc-like structure (Dultzin-Hacyan et al. 2000; Bon et al. 2009) surrounding the accretion disc itself. The matter in BLRs moves at near-virial velocities possessing at the same time large net orbital momentum that is comparable to Keplerian orbital momentum. Until recently, the existence and direction (inflows or outflows) of net radial motions in BLR were debated. However, recent velocity-resolved reverberation mapping results support the existence of an inflow in BLRs of many AGNs (Doroshenko et al. 2012; Grier et al. 2013). Besides, the long-lasting problem of blueshifted high-ionization broad emission lines (Gaskell 1982) is elegantly explained by scattering inside a converging translucent flow (Gaskell 2009; Gaskell & Goosmann 2013) existing in the inner parts of BLRs.

This new observational evidence allows us to unify the dusty torus surrounding most of the well-studied AGN (Tristram et al. 2012), BLR, and the accretion disc into a single accretion flow, as shown in Fig. 1. Transition from the torus towards the partially ionized gas of the BLR is thought to be connected to dust sublimation at the temperature of about $T_{\text{dust}} \simeq (1 - 2) \times 10^3 \text{ K}$, which is weakly dependent on density (Draine 2003; Nenkova et al. 2008). The source of heating is the radiation of the accretion disc. The broad lines themselves are emitted in a certain range of radii, generally in between the size of the dusty torus and the accretion disc. Together with the evidence for inflow this means that inside certain radius the material emitting in the BLR either enters the accretion disc or at least becomes too hot to manifest itself via ultraviolet lines. Both processes probably work and BLR clouds are gradually heated and destroyed and then precipitate into a thin disc because of energy loss mechanisms (collisions and subsequent cooling). At the same time, the geometry of the BLR inherits the oblate geometry of the torus and thus forms a structure sometimes referred to as a “bird’s nest” (Mannucci et al. 1992).

It follows that there should be ionized gas scattering not only the photons of the broad emission lines but also the radiation of the disc. The distance range for this material is dictated, first, by heating by the disc radiation, and, second, by the cooling processes that lead to formation of the thin accretion disc.

In this paper we show that a geometrically thick scattering inflow with sub-virial radial velocity, which gradually deposits its material into the accretion disc, in fact can explain the basic features of the quasar spatial structure resolved by microlensing, such as larger sizes and weaker dependence on wavelength than predicted by the standard disc model.

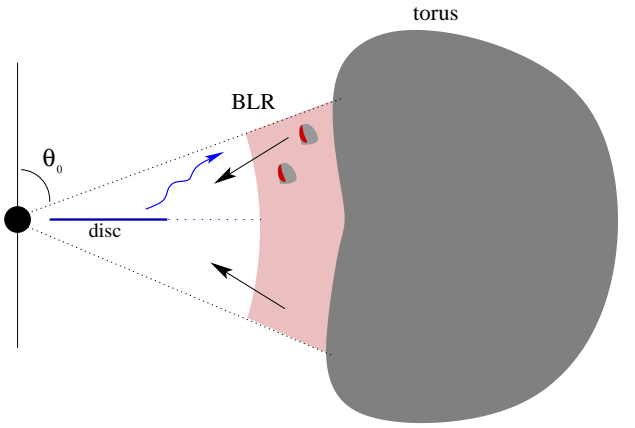


Fig. 1. Sketch illustrating the unified scheme of AGN accretion combining the dusty torus, BLR and accretion disc. Radiation from the accretion disc ionizes and destroys the dusty clouds of the torus and makes them radiate in broad emission lines. The material from the torus and BLR finally precipitates into the disc. A couple of BLR clouds are shown schematically with one side highlighted to indicate the photoionization of the illuminated side of the cloud.

In Sect. 2, we construct a model of the ionized inflow. Intensity distributions for different parameter sets and half-light radii are calculated in Sect. 3. In Sect. 4, our results are compared to observational data. We discuss the results in Sect. 5.

2. Accretion flow structure

We assume that the gas accretes at the total rate of \dot{M} from the gaseous torus in the form of individual optically thick clouds that are subsequently destroyed by disc radiation and mutual interactions. We assume that the radial velocity (directed inward, taken by absolute value) scales with the local virial velocity

$$v_r = \beta \sqrt{\frac{GM}{R}}, \quad (2)$$

where $\beta < 1$ is a dimensionless coefficient. The existing net radial velocity estimates for BLR are sub-virial (Gaskell & Goosmann 2013) by a factor of several, close to but smaller than the chaotic velocities observed in BLRs and responsible for the virial factor of $f_v \sim 5.5$. Virial factor is defined as the ratio of the virial velocity squared to the measured velocity dispersion, $f_v = \frac{GM}{R\langle v^2 \rangle}$ (see for example Park et al. 2012 and references therein). Random motion velocities of BLR clouds are sub-virial by a factor of $1/\sqrt{f_v} \sim 0.4$ and the radial inflow velocities measured for Seyfert galaxies (Doroshenko et al. 2012) are a factor of several smaller, which implies $\beta \sim 0.1$. As we see below in Sect. 4, the likely value of the relative velocity is smaller, of the order 0.01, but in Sect. 3 we adopt $\beta = 0.1$.

We express the mass accretion rate in the disc as $f_d(r)\dot{M}$. All the rest $(1 - f_d)\dot{M}$ is assumed to exist in the form of a geometrically thick highly inhomogeneous flow subtending some solid angle $\Omega = 4\pi \cos \theta_0$, where θ_0 is the half-opening angle of the flow (see Fig. 1), which we hereafter consider fixed. The density of the geometrically thick flow is written as

$$\rho = \frac{(1 - f_d)\dot{M}}{\Omega v_r R^2}. \quad (3)$$

This estimate does not include clumping effects, which are of little importance, as long as scattering is a linear process in density.

In appendix A, it is shown that scattering opacity becomes sensitive to clumping only if the optical depths of individual clumps become considerably large.

Normally, BLR clouds are assumed to have hydrogen column densities of $10^{22} - 10^{24} \text{ cm}^{-2}$, which makes them optically thin to Thomson scattering. These values are relevant for ionized gas; the amount of neutral gas is more difficult to constrain. Total line luminosities together with some limit on the total covering factor allow us to estimate the thickness of the cloud to be close to 10^{23} cm^{-2} (see for instance Peterson 1997, 2006). However, these estimates are biased by the presence of neutral gas and the real column densities may be larger, although there are no indications that these densities should be larger. There are indications (Maiolino et al. 2010) for the existence of a population of cometary-shaped clumps that are visible through X-ray absorption and probably identical to the population of BLR clouds or at least a large part of it. The column densities of these objects are estimated as $10^{23} - 10^{24} \text{ cm}^{-2}$.

In case of optically thick clouds, the effective optical depth is reduced by about the characteristic optical depth of a cloud. Here, clumping was taken into account as a correction multiplier for optical depths $\xi = (1 - e^{-\tau_1})/\tau_1$, where τ_1 is the optical depth of an individual cloud. Dependence of the observed intensity distributions upon clumping is also addressed in Sect. 3.1. Below, the limit of $\tau_1 \rightarrow 0$ is used everywhere by default.

It is instructive to introduce dimensionless quantities

$$r = \frac{Rc^2}{GM}, \quad (4)$$

and \dot{m} according to (1), and the opacity is set to $\kappa \simeq 0.34 \text{ cm}^2 \text{ g}^{-1}$, which is the Thomson scattering opacity (for solar metallicity). Then the density becomes

$$\rho = \frac{4\pi(1-f_d)\dot{m}}{\Omega} \frac{c^2}{\beta} \frac{1}{GM\kappa} r^{-3/2}. \quad (5)$$

The optical depth to scattering in vertical direction is

$$\tau_v(r) \simeq \int_0^{R \cos \theta_0} \kappa \rho dz = \frac{1-f_d}{\beta} \frac{\dot{m}}{\sqrt{r}}. \quad (6)$$

There is one unknown quantity left in our problem, $f_d = f_d(r)$. We consider that radial and vertical motions both scale with the virial velocity and the scattering clouds are destroyed while passing through the equatorial plane. As we show later in Sect. 5.3, the column density of the disc is many orders of magnitude larger than that of a single cloud, therefore BLR clouds should be strongly affected by passage through the accretion disc if the latter has already formed at the radius under consideration. The geometrically thick flow is then depleted as

$$\frac{d}{dR} ((1-f_d)\dot{M}) = 4\pi R \rho v_\theta, \quad (7)$$

where the vertical velocity is also considered virial $v_\theta = \beta_\theta \sqrt{GM/R}$ with $\beta_\theta = \beta$ (for simplicity). The partial mass accretion rate itself, according to (5), equals $(1-f_d)\dot{M} = \Omega R^2 \rho v_r$, hence,

$$\frac{d(1-f_d)}{dR} = \frac{4\pi\beta_\theta}{\Omega} \frac{1-f_d}{R}. \quad (8)$$

This implies a power-law dependence on the radius

$$f_d(r) = 1 - \left(\frac{R}{R_{\text{out}}} \right)^a, \quad (9)$$

where $a = \frac{\beta_\theta}{\beta} \frac{1}{\cos \theta_0} = \frac{1}{\cos \theta_0}$, R_{out} is the outermost radius where accretion disc exists or, alternatively, the outermost radius where the geometrically thick inflow starts to deplete. Outside R_{out} , $f_d = 0$. For simplicity, we assume here the outer radius of the disc equals the outer radius of the ionized flow as well. The radial optical depth of the scattering flow is then

$$\tau_r = \int_{r_{\text{in}}}^r \kappa \rho(r) dr \simeq \frac{4\pi}{(a-1/2)\Omega} \frac{\dot{m}}{\beta} \frac{r^{a-1/2}}{r_{\text{out}}}. \quad (10)$$

Here, r_{in} is the inner radius of the disc. In our assumptions, $a \geq 1$ and thus the lower integration limit is relatively unimportant, especially if $r_{\text{out}} \gg r_{\text{in}}$. The outer radius R_{out} should be a physically motivated quantity that is connected to the processes that lead to destruction of the torus clouds and are responsible for radial drift. The actual value of R_{out} is determined by the radiation fields that destroy dust and ionize the gas composing the clouds. Ionization is the key process because the most relevant process is scattering by free electrons.¹ Large density contrasts and complex geometry make it impossible to estimate the outer radius as the size of the Strömgren region. The only clear and simple criterion that can be used in this case is the radiation density temperature of the radiation of the disc. We assume that the outer radius of the ionized inflow is determined by some radiation energy density temperature T_{out} ,

$$\frac{4\sigma_{\text{SB}}}{c} T_{\text{out}}^4 = \frac{L}{4\pi R^2}, \quad (11)$$

$$r_{\text{out}} = \sqrt{\frac{c^5 \eta \dot{m}}{GM \kappa \sigma_{\text{SB}} T_{\text{out}}^4}} \simeq 10^3 \left(\frac{10^4 \text{ K}}{T_{\text{out}}} \right)^2 \sqrt{\eta \dot{m} \frac{10^9 M_\odot}{M}}. \quad (12)$$

Here, η is radiative efficiency of the accretion disc, which we later assume is equal to 0.057 in all numerical estimates, as for a Schwarzschild black hole. This condition is similar to the dust evaporation condition defined by energy density temperature $T_{\text{ED}} = T_{\text{dust}} \simeq (1-2) \times 10^3 \text{ K}$ (Draine 2003). The proposed limit T_{out} should be not lower than T_{dust} because dust efficiently absorbs EUV radiation and shields the gas from the source.

Total radial optical depth is calculated using expression (10) evaluated at $r = r_{\text{out}}$,

$$\begin{aligned} \tau_r(r_{\text{out}}) &= \frac{4\pi}{(a-1/2)\Omega} \frac{\dot{m}}{\beta} \frac{1}{\sqrt{r_{\text{out}}}} \\ &\simeq \frac{0.03}{(a-1/2)\cos \theta_0} \frac{\dot{m}^{3/4}}{\beta \eta^{1/4}} \left(\frac{M}{10^9 M_\odot} \right)^{1/4} \frac{T_{\text{out}}}{10^4 \text{ K}}. \end{aligned} \quad (13)$$

A fraction of about $\tau_r \Omega / 4\pi$ of the disc luminosity is captured by the inflow and may contribute to the observed radiation of the disc. This quantity may be considerably high even for $\dot{m} \lesssim 1$ depending on β and the radial extent of the scattering region.

3. Observed intensity distribution

We consider the observed intensity distribution composed of two parts: directly visible accretion disc radiation and accretion disc radiation scattered by the inflow. Accretion disc radiation conforms more or less to the standard disc model

¹ Rayleigh scattering is also expected to be important in BLR clouds; see Gaskell & Goosmann (2013). Scattering by dust may be of importance at larger distances because dust albedo is still high, about 0.5, in the far ultraviolet according to observational data and most popular interstellar dust models (see Draine (2003) and references therein).

(Shakura & Sunyaev 1973), but the mass accretion rate becomes smaller at large radii, $\dot{M}_d = f_d \dot{M}$. Besides, at large radii the radiation of the disc is seen through the scattering material. The disc is assumed to be observed at the inclination of i , while the effects of inclination are neglected for the scattered radiation. Below we assume $\cos i = 1$ (disc seen face on) if not stated otherwise. Propagation of the photons scattered by the outer scattering flow is difficult to treat exactly, hence, we consider that some fraction of the disc monochromatic luminosity (primarily the radiation initially going at large inclinations, which have a large probability to be scattered in the inflow) is scrambled and redistributed over the radial coordinates. Finally, monochromatic intensity may be expressed in the form,

$$I_v = I_v^{\text{disc}} e^{-\tau_v \xi} \cos i + (1 - e^{-\tau_v \xi}) \frac{f L_v}{4\pi^2 R^2}, \quad (14)$$

where τ_v is the vertical optical depth calculated according to (6), $\xi = (1 - e^{-\tau_1})/\tau_1$ is clumping correction factor (τ_1 is the optical depth of a single cloud; see Appendix A), $f \simeq \cos \theta_0$ is the luminosity fraction scattered inside the inflow ($f = \cos \theta_0$ for an isotropic source and $f = \cos^2 \theta_0$ for a flat disc without limb darkening; relativistic effects also distort the angular distribution of the radiation of the inner parts of the disc), L_v is the cumulative luminosity of the disc released inside current radius

$$L_v = 4\pi^2 \int_0^R I_v^{\text{disc}} R' dR', \quad (15)$$

an additional π multiplier originating from the transition between flux and intensity, and the local disc intensity is defined by the standard disc theory as the local Planck radiation with the temperature determined by the energy release in the disc, given here according to Shakura & Sunyaev (1973) as follows:

$$I_v^{\text{disc}} = \frac{2h\nu^3}{c^2} \frac{1}{\exp(h\nu/kT(R)) - 1}, \quad (16)$$

$$T(R) \simeq \left(\frac{3}{2} \frac{c^5}{\sigma_{\text{SB}} \kappa GM} \dot{m} \right)^{1/4} \left(1 - \sqrt{\frac{r_{\text{in}}}{r}} \right)^{1/4} \times r^{-3/4} f_d^{1/4}. \quad (17)$$

This expression is for a standard, non-relativistic accretion disc with a mass accretion rate modified by the factor f_d . If the dimensionless mass accretion rate becomes more than about several tens, the accretion disc may become super-Eddington in its inner parts (Poutanen et al. 2007). In this case, the innermost parts of the disc are covered by another scattering envelope that we found, in Abolmasov & Shakura (2013), to be too small, for reasonably low accretion rates, to explain the observational data.

The photon flux from the disc as seen by the scattering medium should also be attenuated by a factor of $e^{-\tau_v \xi}$. However, the scattered radiation has a large (of the order of f) probability to be scattered once more. Multiple scatterings effectively make the radiation isotropic, eventually reproducing the inverse-square scaling with distance, hence we neglect this multiplier and assume that the emissivity of the scattered radiation decreases simply $\propto R^{-2}$. The real intensity distribution should be of course more complicated.

Sample intensities are shown in Figs. 2 and 3 for two different mass accretion rates ($\dot{m} = 1$ and $\dot{m} = 100$) and three different photon frequencies. Depending on the model parameters, spatial properties may be different, but the two-component structure holds for a very broad range of mass accretion rates and outer temperatures. After introducing the scattering component, radius dependence on wavelength always becomes shallower. At larger

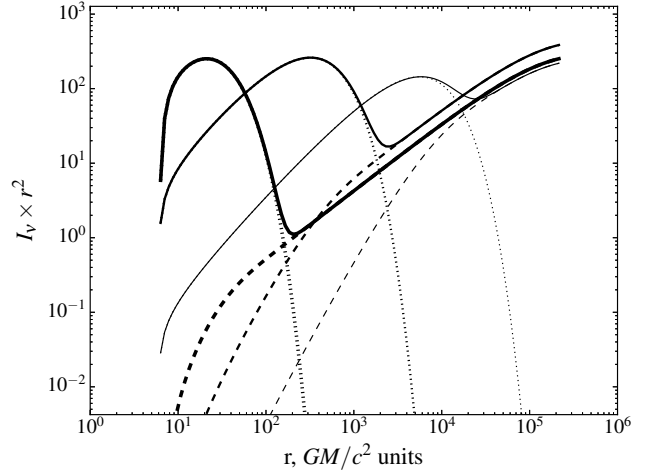


Fig. 2. Intensity (multiplied by r^2 , in relative units) as a function of radius for $\theta_0 = 45^\circ$, $\dot{m} = 100$, $M_{\text{BH}} = 10^8 M_\odot$, $T_{\text{out}} = 10^3 \text{ K}$, and $\beta = 0.1$, $i = 0$ (disc is seen face-on). Three different energies were considered, 0.1, 0.3, and 1 Ry (from the thinnest to the thickest curves). Solid lines show observed (face-on) intensity distributions, dotted lines correspond to standard disc intensity distribution, and dashed lines to the contribution of the scattered radiation.

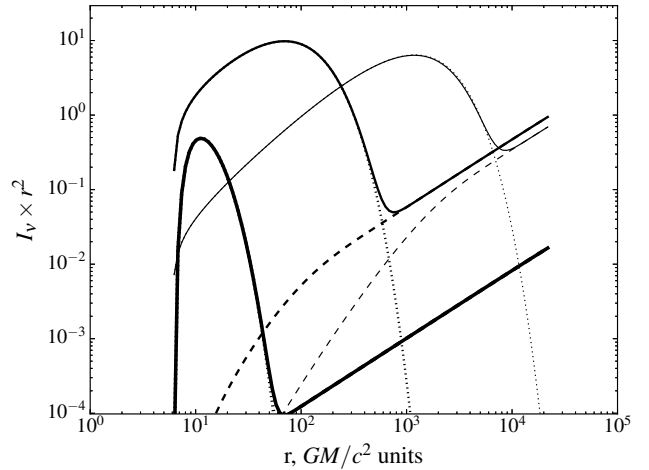


Fig. 3. Same as previous figure, but for $\dot{m} = 1$.

BH masses, the inner and outer edges of the disc set a limit for disc size variations that is independent of the scattering component. At higher dimensionless mass accretion rates, the optical depth of the outer flow becomes large and the contribution of the scattered radiation becomes important. In this latter case, the effective size of the disc increases if the scattered luminosity becomes comparable to the visible luminosity of the disc.

3.1. Apparent disc radius

The quantity primarily responsible for microlensing properties of a source is its half-light radius $R_{1/2}$ inside which half of the observed flux is emitted (Mortonson et al. 2005),

$$\frac{1}{2} = \frac{\int_0^{R_{1/2}} I R dR}{\int_0^{+\infty} I R dR}. \quad (18)$$

This parameter may be contrasted to another quantity that is more convenient for analytical estimates and much more sensitive to scattered light contribution, namely to the intensity-weighted mean radius,

$$\langle R \rangle = \frac{\int_0^{+\infty} IR^2 dR}{\int_0^{+\infty} IR dR}. \quad (19)$$

Two quantities may differ severely if the intensity distribution has extended wings. Half-light radius is actually a non-linear median estimate, which practically ignores wings in intensity distribution if their contribution to the flux is small. At the same time, the mean radius may be affected even by a very faint extended halo. This is well illustrated by Fig. 4 where the mean radius is strongly increased by the existence of faint scattering wings while the half-light radius remains practically unaffected if the mass accretion rate is small ($\dot{m} \lesssim 1$). In Fig. 5, identical quantities are plotted for inclination $i = 60^\circ$. In this case, accretion disc contribution is two times smaller and the effective radii are larger for large mass accretion rates. We do not consider here the contraction of the apparent disc size due to projection effects.

For the intensity distribution introduced above (Eq. 14), one can estimate the effective mean radius in assumption of $\tau_\nu \gg 1$ and L_ν independent of distance,

$$\langle R \rangle = \frac{\langle R \rangle_0 L_\nu + f (R_{\text{out}} - R_{\text{in}}) \times L_\nu}{(1 + f) L_\nu} \simeq \langle R \rangle_0 + f R_{\text{out}}, \quad (20)$$

where $\langle R \rangle_0$ is the half-light radius of an accretion disc without a scattering halo.

At the same time, it may be shown that whenever the half-light radius considerably exceeds the half-light radius of the accretion disc R_d , it should scale approximately as $\sqrt{R_{\text{out}} R_d}$. Indeed, approximating the expression for intensity as $I_\nu^{\text{disc}} + f L_\nu / R^2$, one can re-write the definition of the half-light radius (18) as

$$\int_0^{R_{1/2}} I_\nu^{\text{disc}} R dR + f \frac{L_\nu}{4\pi^2} \ln \left(\frac{R_{1/2}}{R_d} \right) = \frac{1}{2} \frac{L_\nu}{4\pi^2} \cdot \left(1 + f \ln \left(\frac{R_{\text{out}}}{R_d} \right) \right). \quad (21)$$

The R_d limit here arises from the cumulative nature of the luminosity L_ν , which makes the scattering term vanish at the radii smaller than R_d . Finally, one can re-write this condition as

$$\int_0^{R_{1/2}} I_\nu^{\text{disc}} R dR = \frac{1}{2} \frac{L_\nu}{4\pi^2} \cdot \left(1 + f \ln \left(\frac{R_{\text{out}} R_d}{R_{1/2}^2} \right) \right). \quad (22)$$

Because the expression on the left should be larger than $\int_0^{R_d} I_\nu^{\text{disc}} R dR = \frac{L_\nu}{8\pi^2}$, the radius $R_{1/2}$ can not exceed the geometric mean $\sqrt{R_d R_{\text{out}}}$. If the contribution of the halo becomes important and intensity behaves as $I_\nu \propto R^{-2}$, the half-light radius approaches the geometrical mean of some effective inner radius and the outer radius R_{out} ,

$$R_{1/2} \simeq \sqrt{R_d R_{\text{out}}}. \quad (23)$$

There are two important outcomes of this estimate. Firstly, the radius scales with wavelength as $R_{1/2} \propto \lambda^{2/3}$ in this limit. Dependence on wavelength becomes even shallower as the disc radius becomes comparable to R_{out} . Second, $R_{1/2}$ exceeds R_d only if f and R_{out} are large enough. The scattered flux fraction $\sim \cos \theta_0 / \cos i$ depends on the geometrical thickness of the flow and on the inclination of the disc.

Clumping effects make the scattering medium more transparent thus decreasing the scattered fraction of radiation but increasing the mean radius of the halo. Sometimes it leads to a non-monotonic dependence of radius correction factor upon the wavelength. Effects of the optical depth of a single cloud τ_1 are shown in Fig. 6 for two different outer temperatures. Generally, increase in τ_1 decreases the contribution of the scattered radiation, but the effect becomes profound only for $\tau_1 \gg 1$ and scales inversely proportional to τ_1 for large optical depths.

4. Numerical estimates and comparison to observations

We use observational accretion disc sizes and structure parameters to check the validity of the model and constrain its parameters.

4.1. Dependence on wavelength

We parameterize the dependence of the half-light radius on wavelength as $R_{1/2} \propto \lambda^\zeta$ and calculate the values of ζ in the relevant (“big blue bump”) wavelength range $0.1 - 1 \mu\text{m}$. Outside this wavelength range, the accretion disc is likely not the primary radiation source. Shorter wavelengths may be also affected by the relativistic effects and super-Eddington accretion regime in the inner disc parts. For an infinite standard disc (without any outer or inner limits), $\zeta = 4/3$, but several processes, including those considered in the current work, make this quantity lower. In Fig. 7, the estimated values of ζ are compared to the values obtained by fitting the observational data of Blackburne et al. (2011). We set $\beta = 0.01$ because this value allows us to explain the apparent accretion disc sizes (see Sect. 4.2). In each panel, the temperature is fixed and each of the curves corresponds to a fixed physical mass accretion rate.

Several observational radius estimates for different wavelengths between 0.1 and $1 \mu\text{m}$ were used to make the power-law fits shown by black crosses. The power-law slopes best fitted to the observational data were presented in Abolmasov & Shakura (2012). The real shapes of the $R(\lambda)$ dependences are more complex than a true power law, usually showing flattenings at higher and lower wavelengths similar to those expected for an accretion disc model with finite outer and inner edges (see Figs. 6-8 in Blackburne et al. 2011). The average slopes of these curves are often close to zero but still positive and, in a couple of cases, they are very close to the slope of a standard disc.

The mass accretion rate in the outer parts of the disc is probably determined by external processes and thus does not depend on the mass of the black hole. If the mass accretion rate in physical units \dot{M} does not depend on the black hole mass M , dimensionless mass accretion rate scales inversely proportional to the mass $\dot{m} \propto M^{-1}$, and the effects of scattering and distorted intensity distribution become more important for smaller black holes (since the inflow optical depth for a smaller black hole mass is higher; see equation (13)). In Fig. 7, we attempt to reproduce the $M - \zeta$ plot with a population of black holes accreting at fixed mass accretion rate (from 1 to $100 M_\odot \text{ yr}^{-1}$) for different outer temperatures. Using an outer temperature value about $(1 - 3) \times 10^3 \text{ K}$ and dimensional mass accretion rates in the range $3 - 10 M_\odot \text{ yr}^{-1}$ allows us to explain the overall behaviour of the $\zeta - M$ plot. Lower mass supermassive black holes appear in a moderately super-Eddington regime ($\dot{m} \gtrsim 100$, at least several times larger than the critical mass accretion rate), and for these black holes outflows can also affect the properties of the disc.

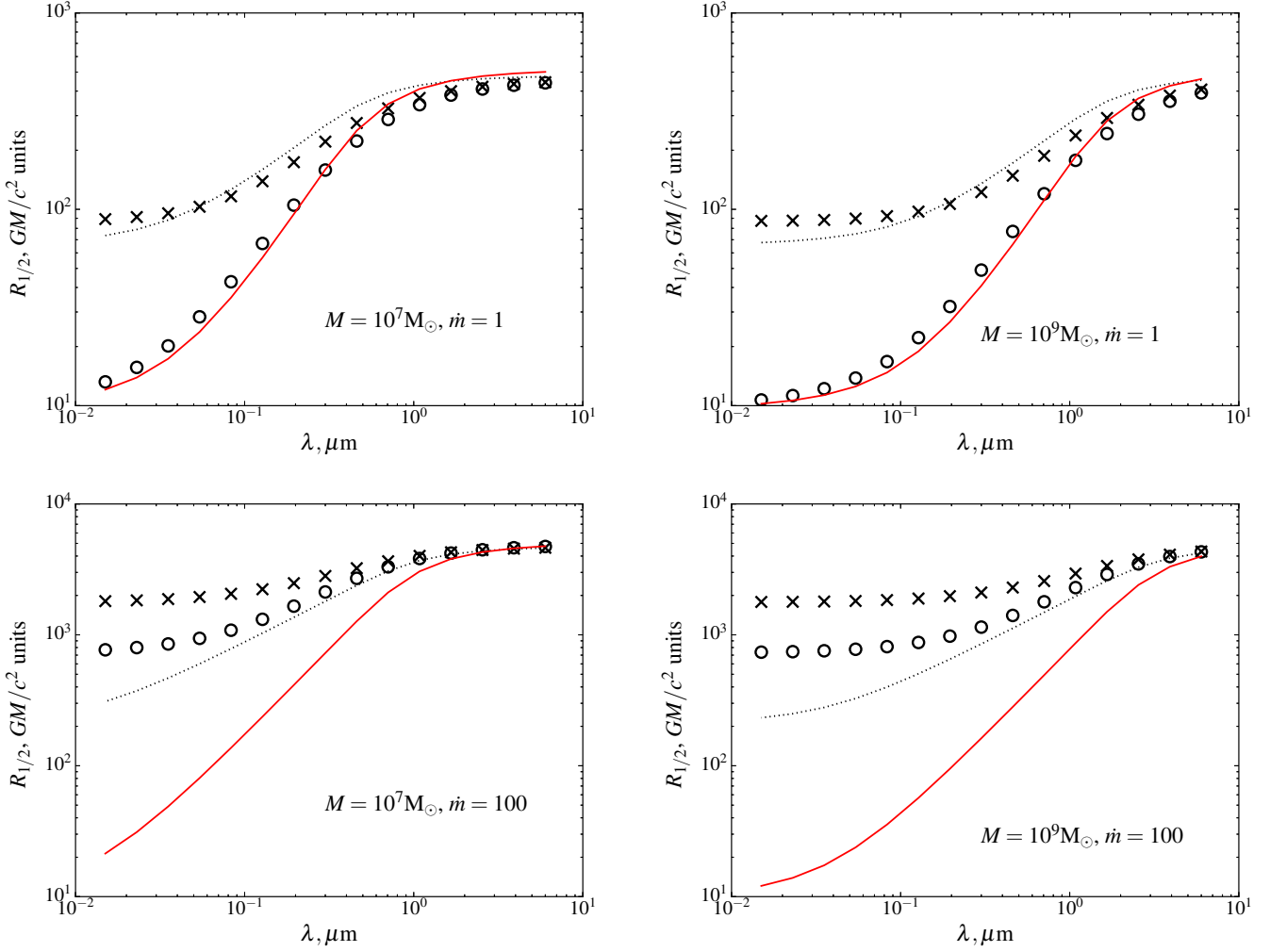


Fig. 4. Half-light radii (open circles) and intensity-weighted mean radii (crosses) for $\theta_0 = 45^\circ$, $T_{\text{out}} = 5 \times 10^3 \text{K}$, and $\beta = 0.1$. BH masses are $10^7 M_\odot$ (left panels) and $10^9 M_\odot$ (right panels). Dimensionless mass accretion rates are $\dot{m} = 1$ (upper panels) and 100 (lower panels). Standard accretion disc predictions are plotted with red solid lines, dotted lines show approximation $R_{1/2} = \sqrt{R_d R_{\text{out}}}$, where R_d is the half-light radius of a standard accretion disc.

However, the size of the envelope formed by the outflow is expected to be smaller than the scattering region (see Sect. 5.4 for a more detailed discussion).

The dimensionless mass accretion rate enters all the optical depths (equations 6 and 13) in combination \dot{m}/β . Hence, for instance, apparently large mass accretion rates may be mimicked by small radial velocities.

Strong deviations from the standard disc power-law asymptotic occur when the flux from the halo becomes comparable to the visible flux from the disc. This requires a significant percentage of the disc luminosity to be scattered ($f \gtrsim 0.5$, $\dot{m}/\beta \gtrsim 10$). For the heaviest objects of the sample (see Fig. 7), observational ζ seems to marginally exceed the standard disc value. There are several effects that can reproduce large structural parameters $\zeta \simeq 2$, one of which is irradiation. If the radiation of the disc is thermalized instead of scattered, the temperature of thermalized radiation scales with radius as $T \propto r^{-1/2}$, which implies $r \propto \lambda^2$.

4.2. Apparent disc sizes for objects with known fluxes

Additional constraints may be made by considering the objects where mass accretion rates may be estimated independently. We

applied our model to single spectral band accretion disc size measurements made by Morgan et al. (2010). The advantage of these data set is the existence of de-lensed fluxes that allow us to make independent mass accretion rate estimates. We consider the sample from Morgan et al. (2010) with the data for one object (Q J0158-4325) replaced by newer data from Morgan et al. (2012), following our work in Abolmasov & Shakura (2012). Mass accretion rate was estimated using monochromatic de-lensed fluxes from Morgan et al. (2010). Standard multi-colour accretion disc approximation allows us to link monochromatic flux (at observer frame $\lambda_{\text{obs}} = 0.79 \mu\text{m}$, which is close to the observable I-band flux) with the mass accretion rate assuming the black hole mass is known. Using expression (9) from Abolmasov & Shakura (2012), we can estimate the mass accretion rate as a function of the observed magnitude of the disc as

$$\dot{m} \simeq 7.4 \times 10^{-4} \left(\frac{10^9 M_\odot}{M} \right)^2 \left(\frac{D_A}{\text{Gpc}} \right)^3 10^{-0.4(I-19)} (1+z)^4 \cos^{-3/2} i, \quad (24)$$

where I is the observed I-band magnitude, z is redshift, and D_A is the angular-size distance (about $1.5 - 1.7 \text{Gpc}$ for all the objects).

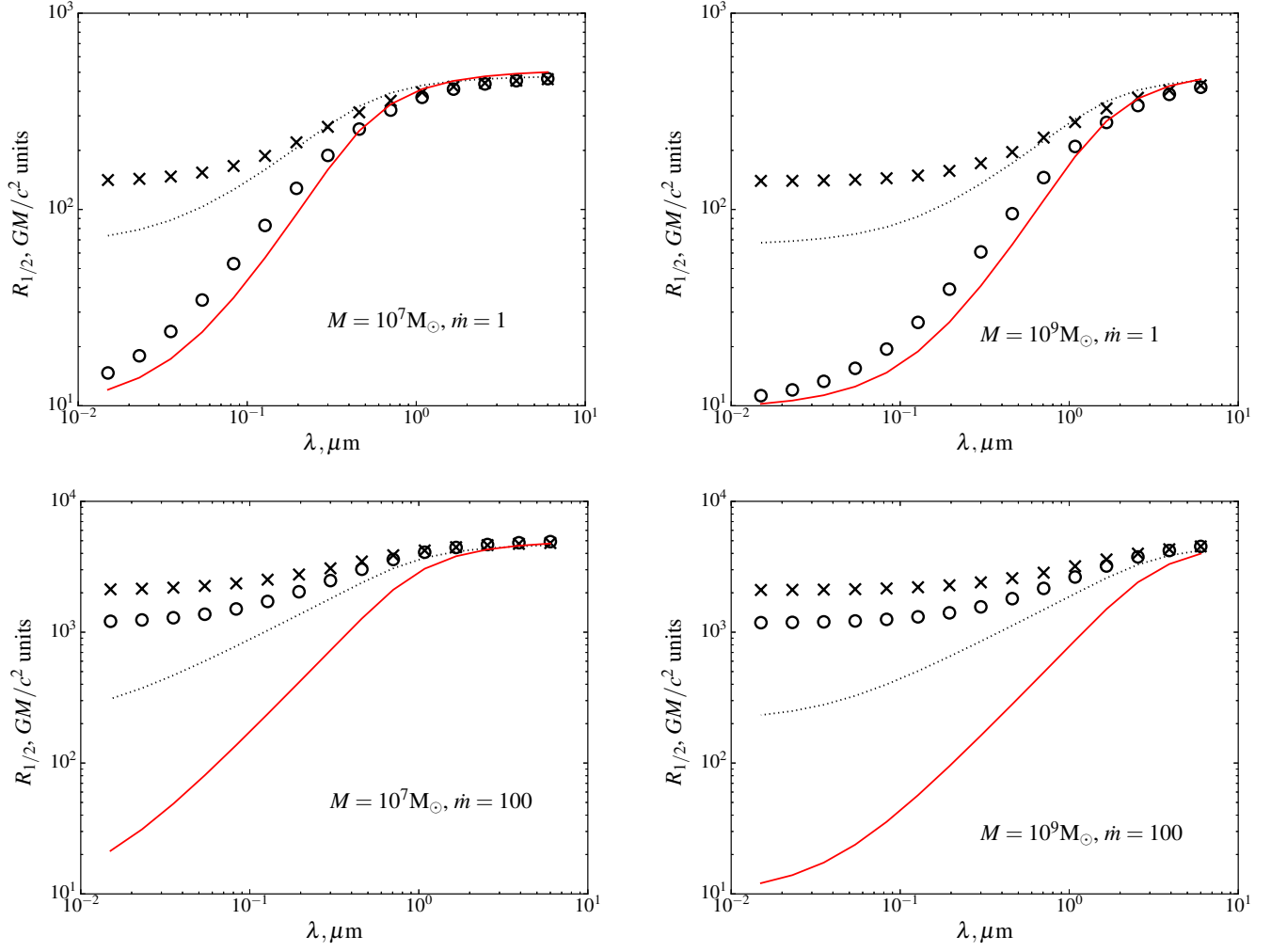


Fig. 5. Same as previous figure, but for an accretion disc inclined by $i = 60^\circ$.

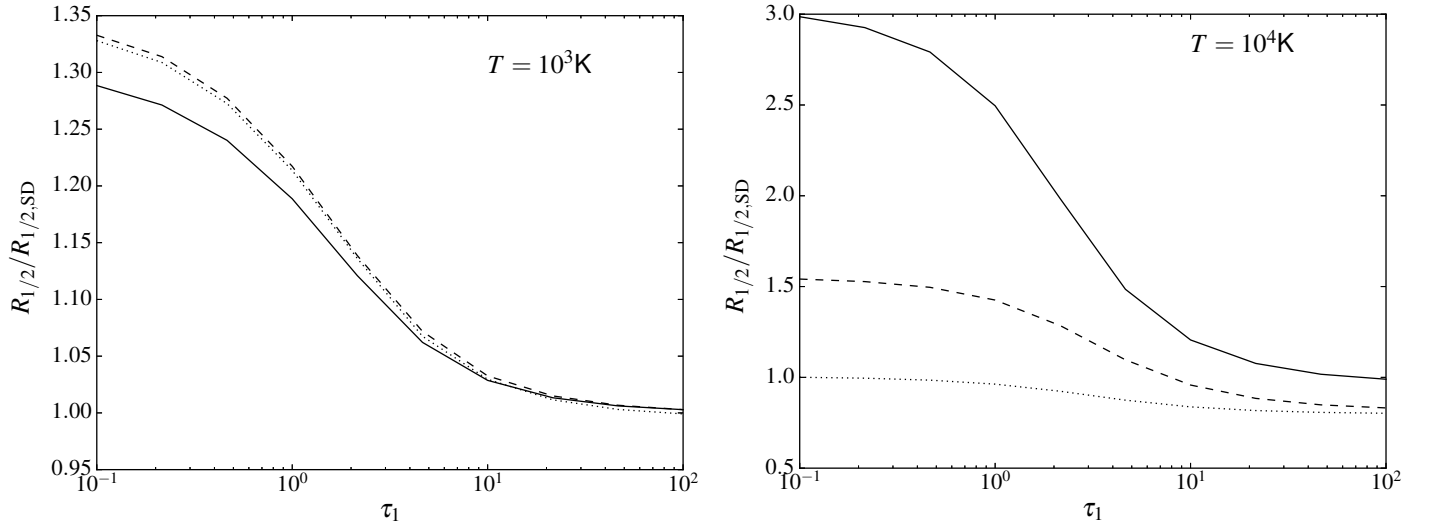


Fig. 6. Half-light radius dependence upon the optical depth of a single cloud for different wavelengths of 0.1 (solid line), 0.3 (dashed), and 1 μm (dotted). Radius is expressed in the units of the standard disc half-light radius at the same wavelength. Black hole mass $M_{\text{BH}} = 10^8 M_\odot$ mass accretion rate $\dot{m} = 10$, temperature limits 10^3 (left), and 10^4 K (right). The disc is seen face-on, $\theta_0 = 45^\circ$.

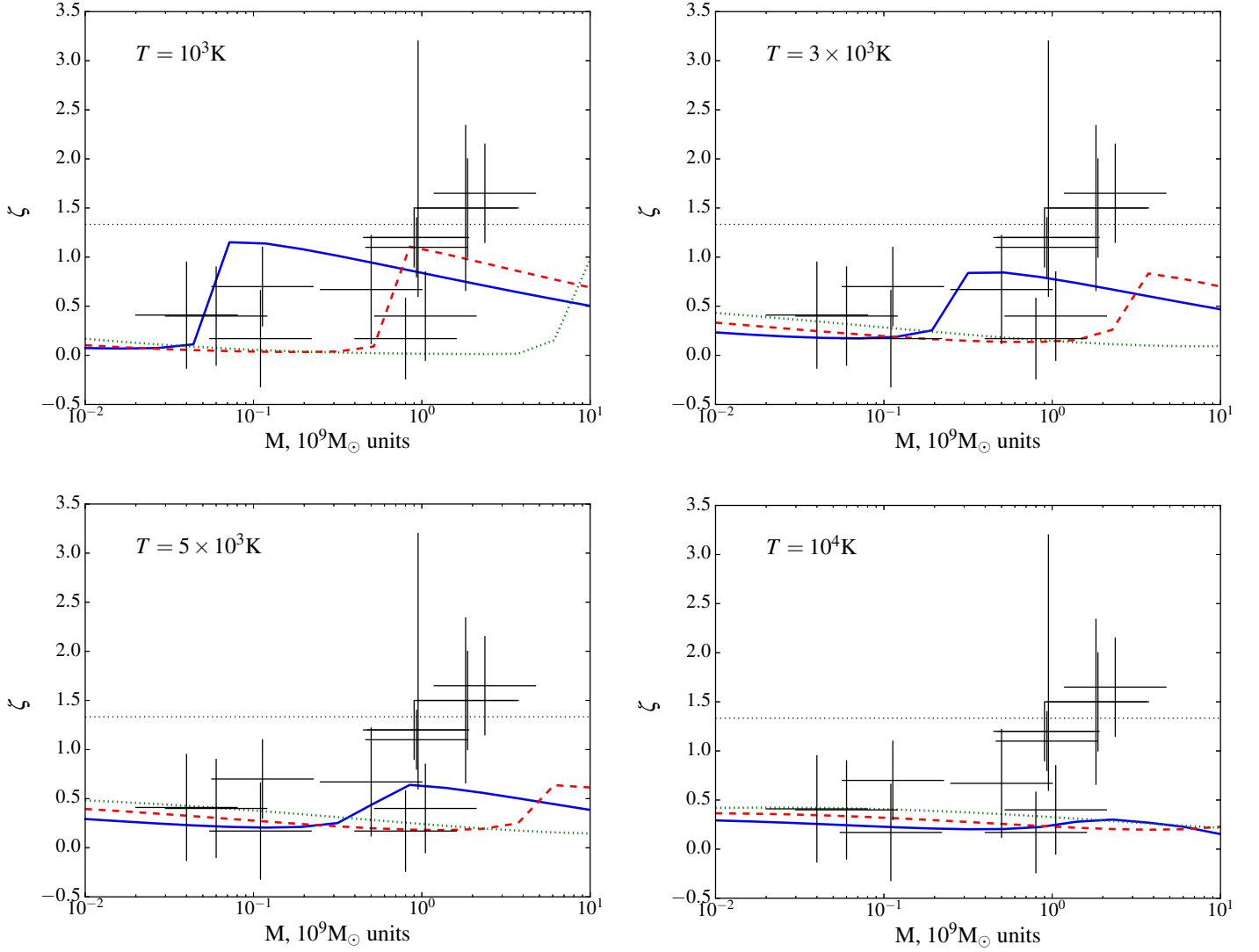


Fig. 7. Comparison of structure parameter ζ estimated from observational data (black crosses) and calculated numerically. Virial mass is shown along the x-axes. From left to right, the outer temperature values are 10^3 , 3×10^3 (upper panels), 5×10^3 , and 10^4 K (lower panels). The three curves in every case correspond to different absolute mass accretion rates (solid blue, dashed red, and dotted green curves correspond to 1, 10, and $100 M_\odot \text{ yr}^{-1}$, respectively). The horizontal dotted line corresponds to the standard disc limit $\zeta = 4/3$. Everywhere the inflow half-opening angle is $\theta_0 = 45^\circ$.

Objects and their basic properties are listed in Table 1. Half-light radii calculated using our model were compared to the observational results using a crude χ^2 criterion,

$$\chi^2 = \sum \left(\frac{\lg R_{1/2} - \lg R_{1/2, \text{model}}}{\Delta \lg R_{1/2}} \right)^2, \quad (25)$$

where the uncertainty $\Delta \lg R_{1/2}$ is half-width of 70% interval in $\lg R_{1/2}$ measured by microlensing effects. Summation was performed for the whole set of 11 objects. We assumed $i = 60^\circ$ and $\theta_0 = 60^\circ$. In Fig. 8, contours of constant χ^2 are overplotted with the shades representing the predicted values of ζ in the spectral range $0.1 - 1 \mu\text{m}$.

The fluxes allow us to estimate the mass accretion rates of $\dot{m} \sim 0.1 - 10$ for the sample of objects, which makes an upper limit for β . As it is shown in Fig. 8, observational data favour $\beta \lesssim 0.1$ and set an upper limit for $T \lesssim 2 \times 10^4$ K. The minimal value of χ^2 is about 1.5 for 9 degrees of freedom that means that the model is over-defined for the existing data, and more com-

prehensive statistical analysis is required in future. However, it also means that observed accretion disc sizes are easily reproduced by a model like ours.

The values of β favoured by our fitting are much smaller than the characteristic velocity dispersions in virial units ($\sim 1/\sqrt{f_v} \simeq 0.4$) known from broad line profiles. Small radial velocity may result from the inefficient angular momentum transport in the inflowing matter. To move inward, the scattering clouds should have some means of angular momentum loss or redistribution. For the case of accretion discs, this is provided by turbulent or magnetic viscosity. We consider several processes possibly responsible for angular momentum transfer in the outer, geometrically thick, part of the flow in Sect. 5.

Lower temperatures $T_{\text{out}} \lesssim 3 \times 10^3$ K make it possible to reproduce different ζ for different objects. As can be seen in Fig. 7, high temperatures restrict the range of possible structure parameters, hence the existence of nearly standard discs in some quasars is naturally reproduced only for $\beta \sim 0.01$, $T_{\text{out}} \sim (1 - 3) \times 10^3$ K.

Table 1. Object set used for fitting in Sect. 4.2. Redshifts z , virial masses M_{vir} , half-light radii $R_{1/2}$, de-lensed I-band magnitudes I_{corr} , dimensionless mass accretion rates, and observed structure parameters ζ_{obs} are given.

Object ID	z	$M_{\text{vir}}, 10^9 M_{\odot}$	$R_{1/2}, 10^{15} \text{cm}$	I_{corr}	\dot{m}	ζ_{obs}
QJ 01584325	1.29	0.16	4.9–19.4	19.09±0.12	2.3–50.5	–
HE 04351223	1.689	0.5	2.4–38.7	20.76±0.25	0.0–1.2	0.1–1.1
SDSS 0924+0219	1.52297	0.11	1.0–4.9	21.24±0.25	0.3–10.1	0.15–0.8
FBQ 0951+2635	1.24603	0.89	12.2–77.2	17.16±0.11	1.0–21.1	–
SDSS 1004+4112	1.73995	0.39	1.0–3.9	20.97±0.22	0.1–1.6	–
HE 11041805	2.3192	2.37	9.7–30.7	18.17±0.31	0.1–4.5	1.65±0.5
PG 1115+080	1.73547	1.23	38.7–193.8	19.52±0.27	0.0–1.2	0.4±0.5
RXJ 11311231	0.654	0.06	3.1–7.7	20.73±0.4	0.2–8.3	0.4±0.5
SDSS 1138+0314	2.44375	0.04	0.5–7.7	21.97±0.19	2.9–79.0	0.4±0.5
SBS 1520+530	1.855	0.88	7.7–19.4	18.92±0.13	0.2–5.3	–
Q 2237+030	1.695	0.9	4.9–19.4	17.9±0.44	0.5–25.7	1.15±0.2

Notes. Except for Q J01584325, all the radii were estimated in Morgan et al. (2010), data for Q J01584325 were taken from Morgan et al. (2012). Mass accretion rates were estimated using the de-lensed flux values of Morgan et al. (2010) in assumption of isotropic emission using formula 24. Structure parameter estimates ζ_{obs} were made by us (Abolmasov & Shakura 2012) using the data by Blackburne et al. (2011).

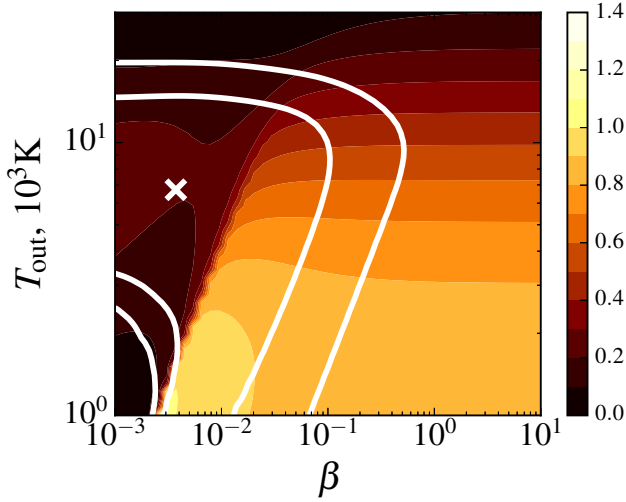


Fig. 8. Structure parameter ζ for a $M = 10^9 M_{\odot}$, $\dot{m} = 1$ disc as a function of β and outer temperature. Overplotted are lines of constant χ^2 (minimal value +2.3 and +4.6, corresponding to 70% and 90% probability if two parameters are varied) for the fitting of disc sizes of the Morgan et al. (2010) sample.

The existence of two populations of quasars, with small and large (about unity) ζ , is then easily explained by roughly universal physical mass accretion rates about $\dot{M} \sim 3 - 30 M_{\odot} \text{yr}^{-1}$ (see Fig. 7).

All these results were obtained for $\theta_0 = 60^\circ$. Smaller solid angles require smaller β , approximately as $\beta \propto \Omega$. It is difficult to put any constraints with the data on hand, but $\Omega \ll 1$ would make it impossible for the scattered component to provide an important contribution. Probability of secondary scatterings is likely to go to zero in this case hence expression (14) is no longer valid, and the secondary (scattered) intensity is limited by the value $\sim \frac{\Omega}{4\pi} I_{\text{v}}^{\text{disc}}$. Therefore, we argue that the solid angle should be large, probably $\frac{\Omega}{4\pi} \gtrsim \frac{1}{2}$, for our model to work.

5. Discussion

5.1. Opening angle and covering factor

For our model, it is important that the scattered flux is comparable or exceeds the primary flux from the accretion disc. This requires a large covering factor of the scatterer, $\frac{\Omega}{4\pi} \gtrsim \frac{1}{2}$.

The geometry of dusty tori was studied for different kinds of AGN, mainly obscured Seyfert galaxies, in several papers (Ibar & Lira 2007; Ichikawa et al. 2015). The estimated half-opening angles are about 60° . On the other hand, about 50–60% of AGN are obscured (Davies et al. 2015), which again results in $\theta_0 \sim 50 - 60^\circ$.

The vertical structure of a BLR, however, does not show any single characteristic opening angle. For instance, Kollatschny & Zetzl (2013) study the geometry of the region in different lines for several nearby well-studied Seyfert galaxies. The relative thickness of the region H/R varies from $\sim 0.1 - 0.3$ for Balmer lines to ~ 1 for hotter lines such as C IV $\lambda 1549$. Although the uncertainties are still very high and the effect is less studied at higher luminosities, it suggests the solid angle of the region is large, possibly larger than the solid angle of the dusty torus. The possible inward increase of the solid angle of the BLR does not necessarily contradict the proposed settling of the material into the disc. If the formation of the disc is driven by cloud collisions, as proposed in Sect. 5.3, some of the matter may be easily brought to orbits with larger inclinations. Besides, radiation and wind from the accretion disc can affect the motion of the clouds through drag and outward pressure. Details of the physics and the interpretation of the observational results are uncertain.

If the radiation of the disc is scattered efficiently, it is geometrically channelled in a solid angle $4\pi - \Omega$, which means that the observed scattered flux is enhanced by the factor of $\sim \left(\frac{4\pi}{\Omega} - 1\right)^{-1}$. This becomes important for $\theta \lesssim \pi/3$, when the amplification factor is about two. We did not consider this effect as it relies on the unknown beaming pattern of the radiation of the disc and exact geometry of the scattering region.

5.2. Mass accretion rates

As we have already shown, the half-light radius starts deviating from that of the disc if the scattered flux becomes comparable to the flux from the disc. The scattered fraction is roughly $\frac{\Omega}{4\pi}\tau_r$, where τ_r is given by (13), and becomes around unity when dimensionless mass accretion rate reaches the critical value

$$\dot{m}_{\text{cr}} \simeq 100 \left(a - \frac{1}{2}\right)^{4/3} \left(\beta \frac{10^4 \text{K}}{T_{\text{out}}}\right)^{4/3} \eta^{1/3} \left(\frac{M}{10^9 M_{\odot}}\right)^{-1/3}. \quad (26)$$

For realistic values of $\beta \sim 0.01$, $T \simeq 10^3 \text{K}$, $a - \frac{1}{2} \simeq 1$, $\eta \simeq 0.06$, and $M \sim 10^9 M_{\odot}$ the critical mass accretion rate $\dot{m}_{\text{cr}} \simeq 2$. More detailed calculations presented in Sect. 4 support this estimate. Adjusting the free parameters β , T_{out} , and a (or the solid angle of the flow, as $a \simeq \cos^{-1} \theta_0$) allows us to shift the critical value in broad limits, where the most probable value is around unity. However, large \dot{m} cannot be excluded either.

Evidently, $\dot{m} \gtrsim 100$ produces a luminosity of $\gtrsim 100\eta \sim 10$ in Eddington units, which makes the accretion disc supercritical in its inner parts. The region of the disc where the local Eddington limit is violated is restricted by the spherization radius $r_{\text{sph}} \simeq \frac{3}{2}\dot{m}$ (Shakura & Sunyaev 1973; Poutanen et al. 2007). On the other hand, the monochromatic half-light radius of the standard accretion disc is, according to Morgan et al. (2010), about 2.44 radial scale lengths, or

$$r_{1/2} \simeq 170 \left(\frac{\lambda}{1\mu}\right)^{4/3} \dot{m}^{1/3} \left(\frac{M}{10^9 M_{\odot}}\right)^{-1/3}, \quad (27)$$

which is either close to or larger than the spherization radius for the parameters we are interested in. Therefore, the effects of disc thickness, advection, and outflows are important mainly for the EUV part of the spectrum $\lambda \lesssim 0.1\mu\text{m}$ that is still poorly covered by microlensing studies. However, if the supercritical part of the disc forms an outflow, the pseudo-photosphere of the outflow may become comparable in size to the accretion disc. We considered this pseudo-photosphere in Abolmasov & Shakura (2012, 2013) and conclude that its contribution can affect the apparent disc size at shorter wavelengths $\lambda \sim 0.1\mu\text{m}$. However, as we show below in Sect. 5.4, the effect of an inflow is generally stronger than that of a supercritical wind.

5.3. Accretion disc formation and interaction with the BLR clouds

In our model, the material is supposed to enter the accretion disc through destruction of BLR clouds. This statement needs some justification. For instance, if the surface mass density of a cloud is much larger than that of the accretion disc, it easily passes through the disc losing only a small portion of its vertical momentum. On the other hand, collision with a high surface density disc leads to significant loss in vertical momentum. Besides, such a collision is highly supersonic and probably leads to destruction of the cloud.

Column number densities of BLR clouds are usually estimated as $N_{\text{BLR}} \sim 10^{23} - 10^{24} \text{cm}^{-2}$ although most of the estimates only constrain the amount of ionized gas and are thus only lower limits (Korista & Goad 2000; Goad & Korista 2015). The surface column density of the accretion disc, on the other hand, may be estimated using the equations of the standard accretion

disc theory (Shakura & Sunyaev 1973) as

$$N_{\text{disc}} \simeq \begin{cases} 7.2 \times 10^{30} \alpha^{-4/5} \dot{m}^{3/5} \left(\frac{M}{10^9 M_{\odot}}\right)^{1/5} r^{-3/5} \text{cm}^{-2}, & r \lesssim 1200 \dot{m}^{2/3}, \\ 2.6 \times 10^{31} \alpha^{-4/5} \dot{m}^{7/10} \left(\frac{M}{10^9 M_{\odot}}\right)^{1/5} r^{-3/4} \text{cm}^{-2}, & r \gtrsim 1200 \dot{m}^{2/3}. \end{cases} \quad (28)$$

The two cases correspond to the so-called zones b and c of the standard disc, differing in dominating opacity sources. The inner radiation-pressure dominated zone a is too compact compared to the size of the BLR. The dimensionless radius r here should be close to the outer radius that we consider in our model or to the empirical size of the BLR that is known to scale approximately as $R_{\text{BLR}} \propto \sqrt{L}$ (Kaspi et al. 2007). The relation given by Kaspi et al. (2007) may be written as

$$R_{\text{BLR}} \simeq 0.2 \sqrt{\eta \dot{m} \frac{M}{10^9 M_{\odot}}} \text{pc}, \quad (29)$$

if one identifies the UV luminosity with the bolometric luminosity $\lambda L_{\lambda}(1350\text{\AA}) \simeq L = \eta \dot{m} L_{\text{Edd}}$. Here, \dot{m} is the dimensionless mass accretion rate (introduced above, see Eq. (1)) and η is the overall accretion efficiency $\eta = \frac{L}{\dot{M} c^2}$. The product $\eta \dot{m} = L/L_{\text{Edd}}$ is also known as the Eddington factor.

In terms of dimensionless radius,

$$r_{\text{BLR}} \simeq 4000 \sqrt{\eta \dot{m} \frac{10^9 M_{\odot}}{M}}, \quad (30)$$

close to the outer radius given by expression (12) for $T_{\text{out}} \simeq 2000\text{K}$.

At this radius, the hydrogen column density in the disc $N_{\text{disc}} \sim 10^{28} - 10^{30} \text{cm}^{-2}$, greatly exceeding the column densities estimated for BLR clouds. Unless all the column densities in BLR are vastly underestimated, the accretion disc easily becomes an impassable barrier for BLR clouds and thus efficiently absorbs their material.

Formation of the seed accretion disc that subsequently drains mass from the BLR may be connected to cloud-cloud interaction. Indeed, for a given spherical cloud of density n and column density N , the number of collisions per second is about

$$\nu_{\text{cc}} \simeq \frac{\pi}{4} \left(\frac{N}{n}\right)^2 v n_{\text{c}}, \quad (31)$$

where n_{c} is the volume density of the clouds, and $v \sim \sqrt{\frac{2GM}{f_{\text{v}} R}}$

is the mean relative collision velocity. The number density of the clouds may be expressed through mass accretion rate, radial velocity, and cloud mass as

$$n_{\text{c}} \simeq \frac{\dot{M}}{4\pi R^2 v_r M_{\text{c}}}, \quad (32)$$

where $M_{\text{c}} \simeq N^3 n^{-2} m_{\text{p}}$ is the mass of a cloud. Neglecting multipliers of the order unity,

$$\nu_{\text{cc}} \simeq \frac{GM\dot{m}}{\beta \sigma_T c R^2 N}. \quad (33)$$

At the empirical BLR radius given by the estimate (29), this frequency becomes

$$\nu_{\text{cc}} \sim 10^{-9} \frac{1}{\beta} \frac{M}{10^9 M_{\odot}} \frac{10^{23} \text{cm}^{-2}}{N} \text{s}^{-1}, \quad (34)$$

that is close to or even higher than the local Keplerian frequency $\Omega_K = \sqrt{GM/R^3} \sim 10^{-9}(M/10^9 M_\odot)^{-1/4}(\eta\dot{m})^{-3/4}\text{s}^{-1}$ meaning that cloud collision is an important process that may be driving the radial flow inside the BLR and formation of the accretion disc.

5.4. Optical depths of inflows and outflows

Whenever a geometrically thick inflow exists, its optical depth should be higher than that of the corresponding outflow for two reasons: (i) the mass ejection rate cannot exceed the mass inflow rate and (ii) the velocity of the outflow should be larger. The second condition requires quantitative estimates. If one considers wind accelerated in a gravitational field of a point mass M at some distance R , most of its velocity is gained near the sonic surface (or some sonic surface analogue if non-thermal processes are responsible for acceleration; see Lamers & Cassinelli 1999), where the velocity of the wind should exceed the local parabolic velocity. Otherwise, the flow remains bound and falls back into the accretion disc; this possibility is also interesting as a possible explanation for the spatial properties of quasar discs. Non-zero terminal velocity of the wind is the result of kinetic energy exceeding the potential energy at the sonic radius. At larger distances, it is practically constant and

$$v_w = \beta_w \sqrt{\frac{GM}{R_s}}, \quad (35)$$

where β_w is some dimensionless constant of order unity and R_s is the sonic radius. We note that $\beta_w \ll 1$ requires fine tuning between the kinetic and potential energy in the wind acceleration region. At the same time, depending on its angular momentum, the radial velocity of an inflow may be close to or much smaller than the virial

$$v_{\text{in}} = \beta \sqrt{\frac{GM}{R}}, \quad (36)$$

where β can be significantly smaller than unity. Difference in velocities implies difference in optical depths by a factor of $\frac{\tau_{\text{in}}}{\tau_w} \sim$

$\frac{\beta_w}{\beta} \frac{\dot{M}}{\dot{M}_w} > 1$. While the optical depths may be comparable, the spatial distributions of the scattering matter are different. If one considers a spherically symmetric density distribution, its optical depth from some radius R to infinity is

$$\tau(R) = \kappa \int_R^{+\infty} \rho dR. \quad (37)$$

Pseudo-photosphere radius R_1 is defined by condition $\tau(R) = 1$. If the velocity is parabolic everywhere,

$$\rho(R) = \frac{\dot{M}}{4\pi R^2 v(R)} = \frac{c^2}{GM\kappa} \frac{\dot{m}}{\beta} r^{-3/2}, \quad (38)$$

which implies $\tau = 2\dot{m}/\beta\sqrt{r}$ and dimensionless radius of the pseudo-photosphere $r_1 = 4\left(\frac{\dot{m}}{\beta}\right)^2$. This may be contrasted to the super-virial outflow case that we consider in Abolmasov & Shakura (2012). Optical depth reaches unity for $r_1 \sim \dot{m}^{3/2}$ for a hyperbolic outflow and for $r_1 \sim \dot{m}^2$ for a parabolic inflow. This allows scattering inflows to produce more extended halos and pseudo-photospheres for identical mass accretion rates as long as they stay sub-virial.

5.5. Dynamics of the inflow

If a significant portion of the radiation of the disc is scattered by a geometrically thick inflow, one can also expect this radiation to have some dynamical effect upon the scattering medium. However, independent of the mass accretion rate, this effect is insufficient to power the angular momentum loss inside the scattering region. Tangential momentum flux carried out by scattered radiation may be calculated as the momentum flux density of the radiation $\frac{L}{4\pi c R^2}$ multiplied by the local tangential velocity in light velocity units v_ϕ/c . Hence the radiation acts upon the scattering medium with the torque

$$K \simeq \frac{\Omega}{4\pi} L_{\text{disc}} \cdot v_\phi R / c^2 \sim \frac{\Omega}{4\pi} \eta \dot{M} \sqrt{GMR}. \quad (39)$$

Here, η is the radiative efficiency of the disc and Ω is the solid angle subtended by the inflow. On the other hand, the angular momentum flux carried by the accreting matter through the same surface of radius R is $\dot{M} \sqrt{GMR} > K$ for any combination of parameters since $\eta < 1, \Omega < 4\pi$. Radiation drag is at least several times short in powering the angular momentum transfer in the inflow.

5.6. Self-consistent mass accretion rate

While radiation of the disc is unable to power angular momentum transfer, this radiation can induce angular momentum transfer by magnetic fields by keeping the matter ionized. If the number of hydrogen-ionizing quanta generated by the disc is Q_H , the ionized mass is $M_g \simeq m Q_H / \alpha_r n_e$. For $Q_H \sim 10^{56} \text{s}^{-1}$, hydrogen recombination coefficient $\alpha_r \simeq 2 \times 10^{13} \text{cm}^3 \text{s}^{-1}$, mean particle mass 0.6 of a proton mass ($m \simeq 0.6 m_p$), and $n_e \sim 10^{11} \text{cm}^{-3}$ (about or somewhat lower than the densities typically estimated for BLRs; see for example Negrete et al. (2012)), the ionized mass is about several solar masses. The estimated BLR masses are much higher owing to incomplete ionization (Baldwin et al. 2003). If all the ionized material moves inward with sub-virial velocities as was assumed here, its mass infall rate is

$$\dot{M}_{\text{in}} \simeq \beta M_g \Omega_K(R_{\text{out}}), \quad (40)$$

where $\Omega_K(R) = \sqrt{GM/R^3}$ is the local Keplerian frequency. Substituting here the above expression for the mass of the ionized gas and expression (12) for the outer radius, one obtains

$$\dot{M}_{\text{in}} \simeq \frac{\beta m Q_H}{\alpha_r n_e} \sqrt{GM} \left(\frac{\kappa \sigma_{\text{SB}} T_{\text{out}}^4}{\eta \dot{m} G M c} \right)^{3/4}. \quad (41)$$

If the inner disc temperature is hotter than one Rydberg (Ry), the ionizing quanta production rate Q_H grows with the mass accretion rate approximately as $Q_H \sim L/\text{Ry} = \eta \dot{M} c^2 / \text{Ry}$. Some part of this value, namely $\Omega/4\pi$, is intercepted by the inflow. Assuming $\dot{M}_{\text{in}} = \dot{M}$, one can obtain an estimate for self-consistent mass accretion rate as follows:

$$\begin{aligned} \dot{m} &\simeq \frac{\eta^{1/3} \kappa \sigma_{\text{SB}} T_{\text{out}}^4}{c (GM)^{1/3}} \left(\frac{\Omega \beta}{4\pi \text{Ry} \alpha_r n_e} \right)^{4/3} \simeq \\ &\simeq 7 \times 10^{-4} \eta^{1/3} \left(\frac{\Omega}{4\pi} \frac{\beta}{0.01} \frac{10^{11} \text{cm}^{-3}}{n_e} \right)^{4/3} \left(\frac{M}{10^9 M_\odot} \right)^{-1/3} \left(\frac{T_{\text{out}}}{10^3 \text{K}} \right)^4. \end{aligned} \quad (42)$$

This estimate means that, for a broad range of parameters allowed by the fitting and estimates made in Sect. 4, the radiation

is insufficient to ionized significant part of the flow. An alternative way to start angular momentum transfer at the regions as far as R_{out} is through cloud collisions that may happen considerably often, as shown in Sect. 5.3.

Partial ionization of the accretion flow also means that pure scattering may not be as important as reprocessing of radiation, as already mentioned in Sect. 4.1. The existence of a preferred radius at which the radiation is reprocessed (close to R_{out} or the radius of the BLR) suppresses the proposed increase in ζ . The measured “disc” radius should instead approach the value of R_{out} at the wavelengths where reprocessed emission dominates. The contribution of reprocessed emission was already proposed to be important for explaining the shape of the quasar “big blue bump” in the UV-to-optical spectral range and may be equally important for understanding its spatial properties (Lawrence 2012).

6. Conclusions

Different sites may be responsible for scattering the radiation of the discs around supermassive black holes. At super-Eddington mass accretion rates, the inner parts of the disc are expected to be covered by the pseudo-photosphere of the disc wind. At the same time, near the outer limits of the disc, partially ionized material associated with BLR or some parts of it may produce a scattering halo. It seems that this effect is even more important for the measured half-light radii. Such a model can explain the observed shallow dependences of the quasar half-light radii on wavelength and the generally larger observed disc sizes. The required mass accretion rates may be close to Eddington, but may be much lower if the inflow velocity is less than or about several per cent of virial. The size of the scattering region should be close to the distance where energy density temperature reaches $T_{\text{out}} \sim (1 - 3) \times 10^3 \text{ K}$, that is close to dust evaporation limit. The covering factor of the inflow should be comparable to unity ($\cos \theta_0 \gtrsim 0.5$) to make the contribution of the scattered emission measurable.

Acknowledgements. Research was supported by Academy of Finland grant 268740 and by Russian Scientific Foundation (RSF) grant 14-12-00146 (clumping corrections to opacity). The author would like to thank Juri Poutanen and Anna Chashkina for discussions.

References

Abolmasov, P. & Shakura, N. I. 2012, MNRAS, 427, 1867
 Abolmasov, P. & Shakura, N. I. 2013, MNRAS, 434, 906
 Baldwin, J. A., Ferland, G. J., Korista, K. T., Hamann, F., & Dietrich, M. 2003, ApJ, 582, 590
 Blackburne, J. A., Pooley, D., Rappaport, S., & Schechter, P. L. 2011, ApJ, 729, 34
 Bon, E., Gavrilović, N., La Mura, G., & Popović, L. Č. 2009, New A Rev., 53, 121
 Collin, S., Boisson, C., Mouchet, M., et al. 2002, A&A, 388, 771
 Davies, R. I., Bartscher, L., Rosario, D., et al. 2015, ApJ, 806, 127
 Doroshenko, V. T., Sergeev, S. G., Klimanov, S. A., Pronik, V. I., & Efimov, Y. S. 2012, MNRAS, 426, 416
 Draine, B. T. 2003, ARA&A, 41, 241
 Dultzin-Hacyan, D., Marziani, P., & Sulentic, J. W. 2000, in Revista Mexicana de Astronomia y Astrofisica, vol. 27, Vol. 9, Astrophysical Plasmas: Codes, Models, and Observations, ed. S. J. Arthur, N. S. Brickhouse, & J. Franco, 308–315
 Floyd, D. J. E., Bate, N. F., & Webster, R. L. 2009, MNRAS, 398, 233
 Gaskell, C. M. 1982, ApJ, 263, 79
 Gaskell, C. M. 2009, New A Rev., 53, 140
 Gaskell, C. M. & Goosmann, R. W. 2013, ApJ, 769, 30
 Goad, M. R. & Korista, K. T. 2015, MNRAS, 453, 3662
 Grier, C. J., Peterson, B. M., Horne, K., et al. 2013, ApJ, 764, 47
 Ibar, E. & Lira, P. 2007, A&A, 466, 531
 Ichikawa, K., Packham, C., Ramos Almeida, C., et al. 2015, ApJ, 803, 57

Kaspi, S., Brandt, W. N., Maoz, D., et al. 2007, ApJ, 659, 997
 Kollatschny, W. & Zetzl, M. 2013, A&A, 558, A26
 Korista, K. T. & Goad, M. R. 2000, ApJ, 536, 284
 Lamers, H. J. G. L. M. & Cassinelli, J. P. 1999, Introduction to Stellar Winds (Cambridge, UK: Cambridge University Press)
 Lawrence, A. 2012, MNRAS, 423, 451
 Maiolino, R., Risaliti, G., Salvati, M., et al. 2010, A&A, 517, A47
 Mannucci, F., Salvati, M., & Stanga, R. M. 1992, ApJ, 394, 98
 Morgan, C. W., Hainline, L. J., Chen, B., et al. 2012, ApJ, 756, 52
 Morgan, C. W., Kochanek, C. S., Morgan, N. D., & Falco, E. E. 2010, ApJ, 712, 1129
 Mortonson, M. J., Schechter, P. L., & Wambsganss, J. 2005, ApJ, 628, 594
 Negrete, C. A., Dultzin, D., Marziani, P., & Sulentic, J. W. 2012, ApJ, 757, 62
 Nenkova, M., Sirocky, M. M., Ivezić, Ž., & Elitzur, M. 2008, ApJ, 685, 147
 Park, D., Kelly, B. C., Woo, J.-H., & Treu, T. 2012, ApJS, 203, 6
 Peterson, B. M. 1997, An Introduction to Active Galactic Nuclei (Cambridge, New York Cambridge University Press)
 Peterson, B. M. 2006, in Lecture Notes in Physics, Berlin Springer Verlag, Vol. 693, Physics of Active Galactic Nuclei at all Scales, ed. D. Alloin, 77
 Pooley, D., Blackburne, J. A., Rappaport, S., & Schechter, P. L. 2007, ApJ, 661, 19
 Poutanen, J., Lipunova, G., Fabrika, S., Butkevich, A. G., & Abolmasov, P. 2007, MNRAS, 377, 1187
 Shakura, N. I. & Sunyaev, R. A. 1973, A&A, 24, 337
 Tristram, K. R. W., Schartmann, M., Bartscher, L., et al. 2012, Journal of Physics Conference Series, 372, 012035
 Yan, C.-S., Lu, Y., Yu, Q., Mao, S., & Wambsganss, J. 2014, ApJ, 784, 100

Appendix A: Radiation extinction by clumpy medium

The outcome of small-scale, but strong inhomogeneities may be illustrated by the following toy model. We consider scattering medium consisting of small identical clouds, each having optical depth τ_1 . We also assume the clouds distributed randomly in space. The number of clouds x encountered by a given light beam on some distance l should have Poissonian distribution

$$P(x) = \mu^x e^{-\mu} / x!, \quad (\text{A.1})$$

where $\mu = n_c A l$ is the expectation for x , n_c is the number density of the clouds, and A is the cross-section of a cloud. If one considers the clouds to be spheres of a single radius R_c ,

$$\mu = n_c \pi R_c^2 l = \frac{3}{4} \frac{F}{R_c} l, \text{ where } F \text{ is the volume fraction (filling}$$

factor) of the clouds. Because $\tau_1 \simeq \frac{1}{F} \sigma n R_c$, where σ is the extinction cross-section, and n is the mean density (hence the density inside a cloud is n/F), the mean optical depth is independent of filling factor,

$$\langle \tau \rangle = \tau_1 \mu = \frac{3}{4} \frac{F l}{R_c} \tau_1 \simeq \sigma n l. \quad (\text{A.2})$$

Up to the factor of order unity, this quantity equals the optical depth of an unclumped medium with identical mean density.

At the same time, the optical depth becomes a stochastic variable because of the randomly distributed number of clouds encountered. Dispersion of the number of clouds equals μ due to the properties of Poissonian distribution, hence for $\mu \lesssim 1$ variations in optical depth are important. Because we are primarily interested in attenuated intensity, it is instructive to estimate the mean value of intensity attenuation factor,

$$\langle e^{-\tau} \rangle = \sum_{x=0}^{+\infty} \frac{e^{-\tau_1 x} e^{-\mu} \mu^x}{x!} = e^{-\mu} \sum_{x=0}^{+\infty} \frac{(e^{-\tau_1} \mu)^x}{x!} = e^{-(1-e^{-\tau_1})\mu}. \quad (\text{A.3})$$

Thus, extinction effectively becomes lower with respect to the case of uniform medium. One can express the above result in terms of effective optical depth

$$\tau_{\text{eff}} = \frac{1 - e^{-\tau_1}}{\tau_1} \langle \tau \rangle. \quad (\text{A.4})$$

Effective optical depth depends only upon the optical depth of a single cloud and evolves from $\langle \tau \rangle$ at small τ_1 to $\sim \langle \tau \rangle / \tau_1$ for high τ_1 ; there is no intrinsic dependence upon the filling factor or cloud size. Smaller effective optical depth is a consequence of the increasingly large probability that a particular line of sight will not hit any cloud.